Charge carriers and small-polaron migration as the origin of intrinsic dielectric anomalies in multiferroic $TbMnO_3$ polycrystals

2013 J. Phys.: Condens. Matter 25 475401

(http://iopscience.iop.org/0953-8984/25/47/475401)

J. Phys.: Condens. Matter **25** (2013) 475401 (8pp) doi:10.1088/0953-8984/25/47/475401

Charge carriers and small-polaron migration as the origin of intrinsic dielectric anomalies in multiferroic $TbMnO_3$ polycrystals

L G D Silveira[1], G S Dias[1], L F Cótica[1], J A Eiras[2], D Garcia[2], J A Sampaio[3], F Yokaichiya[4] and I A Santos[1]

[1] Departamento de Física, Universidade Estadual de Maringá, Avenida Colombo, 5790, Maringá 87020-900, PR, Brazil
[2] Departamento de Física, Universidade Federal de São Carlos, Rodovia, Washington Luiz, km 235, São Carlos 13565-905, SP, Brazil
[3] Laboratório de Ciências Físicas, Universidade Estadual do Norte Fluminense Darcy Ribeiro, Avenida Alberto Lamego, 2000, Campos dos Goytacazes 28013-602, RJ, Brazil
[4] Centro do Reator de Pesquisa, Instituto de Pesquisas Energéticas e Nucleares, Avenida Lineu Prestes, 2242, São Paulo 05508-000, SP, Brazil

E-mail: iasantos@dfi.uem.br

Received 1 July 2013, in final form 30 September 2013
Published 28 October 2013
Online at stacks.iop.org/JPhysCM/25/475401

Abstract
Temperature-dependent and frequency-dependent dielectric investigations have been performed in $TbMnO_3$ polycrystals sintered in either oxidative or reductive atmospheres. The results revealed the occurrence of two dielectric anomalies above 100 K, which are caused by the thermal activation of charge carriers and their motion in grain cores and grain boundaries. The temperature dependence of the bulk dc conductivity was also analysed and indicates that charge carriers move between inequivalent sites according to a variable-range-hopping mechanism. Also, a strong correlation between dielectric properties and crystalline structure was observed. Furthermore, a low-temperature dielectric relaxation, commonly reported in rare-earth manganite crystals, was observed in both samples. This relaxation follows the empirical Cole–Cole model and was attributed to small-polaron tunnelling. Polaron motion was observed to be affected by the magnetic transitions, structural properties and intrinsic anisotropies in $TbMnO_3$. It is also worth mentioning that the dielectric anomaly due to motion of charge carriers in grain boundaries is the only one of extrinsic origin, while the anomalies related to carrier motion in grain cores and small-polaron tunnelling are intrinsic to $TbMnO_3$.

1. Introduction

Magnetism and ferroelectricity are essential to many forms of current technology, and the search for multiferroic materials, where these two phenomena are intimately coupled, is of great technological and fundamental importance [1]. However, these two phenomena tend to be mutually exclusive and interact weakly with each other when they coexist [2]. The control of electric properties by magnetic fields was recently achieved in an unexpected class of materials known as 'frustrated magnets', such as the perovskites $RMnO_3$, RMn_2O_5 (R: rare earths), $Ni_3V_2O_8$, delafossite $CuFeO_2$, spinel $CoCr_2O_4$, $MnWO_4$, and hexagonal ferrite $(Ba, Sr)_2Zn_2Fe_{12}O_{22}$ [3–9]. The reason for the observed high sensitivity of the dielectric properties to an applied magnetic field lies in the magnetic origin of their ferroelectricity, which is induced by complex spin structures [10], characteristic of frustrated magnets.

$TbMnO_3$ (TMO) is one of the rare-earth manganites which exhibits magnetoelectric and magnetocapacitance effects. It presents several magnetic transitions at low temperatures. An incommensurate sinusoidal antiferromagnetic (AFM) ordering of Mn^{3+} moments takes place at ∼41 K, which becomes commensurated at ∼27 K, where the magnetic modulation wavevector is locked at a constant value (lock-in). The incommensurate–commensurate transition is also related to the appearance of ferroelectricity in this material. And, at ∼7 K, the magnetic ordering of Tb^{3+} moments occurs [11]. As first reported by Kimura *et al* [3], a spontaneous electric polarization along the *c*-axis of TMO single crystals is observed below the lock-in temperature. It is generally accepted that ferroelectric polarization is induced by the cycloidal spin ordering, which breaks inversion symmetry [10]. However, three different mechanisms have been considered in order to explain the occurrence of ferroelectricity: magnetoelastically induced lattice modulation [3, 12], inverse Dzyaloshinskii–Moriya interaction [13, 14], and spin current [15]. Furthermore, evidence of magnetoelectric coupling, such as the magnetic-field-induced ferroelectric polarization flop and electric control of spin helicity, was also observed [3, 16], further revealing the magnetically activated origin of the electrical polarization.

In perovskite manganites, one of the most prominent magnetocapacitive effects is a strong anomaly of the temperature-dependent dielectric constant ε' in the vicinity of magnetic transitions. Here, either a steplike behaviour or sharp peaks are observed, the latter being taken as evidence of ferroelectric ordering. These effects arise along the crystallographic **a** and/or **c** directions, but not along **b**. Also, a relaxation behaviour is observed for the electric field direction $\mathbf{E} \parallel \mathbf{c}$. It shows up as a steplike increase of ε', shifting to higher temperatures with increasing frequency [12, 17, 18]. It has been suggested that these relaxations are due the motion of multiferroic domain walls [19, 20], migration of localized charge carriers [12], off-centre motion of Mn ions [18], and the Maxwell–Wagner effect related to isolated impurities [17]. The relation between these anomalies and the magnetic transitions, however, remains disputable. In fact, Park *et al* [17] have argued that the dielectric anomalies should not have a frequency dependency if originating from a magnetic transition. Moreover, these anomalies are observed at temperatures above the ferroelectric transition, making it difficult to attribute them to ferroelectricity, and the fact that those anomalies were observed only along a specific crystallographic direction indicates that they are not due to the inclusion of randomly oriented impurities in the crystals. However, the mentioned studies were mainly focused on single-crystal samples. Concerning microstructural and dielectric inhomogeneity, the dielectric response of polycrystalline ceramics is a rather more challenging open issue. Although there are few dielectric investigations of $TbMnO_3$ [21], $DyMnO_3$ [22], and $DyMn_{1-x}Fe_xO_3$ [23] polycrystals, with the exception of the recent work by Yang *et al* [22], the reported dielectric data were mainly concentrated in the fairly high temperature range above 100 K. Considering the rich physical phenomena at low temperatures, extending dielectric studies to lower temperatures is of fundamental interest. Systematic investigations could help elucidate the correlations between dielectric properties, electrical transport and magnetic ordering, and provide new insights into the nature of magnetoelectric and magnetocapacitive effects in rare-earth manganites.

In this paper we report the results of a detailed temperature-dependent (10–300 K) and frequency-dependent (20 Hz–2 MHz) dielectric investigation on TMO ceramics sintered in either O_2 or Ar atmospheres. The dielectric responses of both samples are due to the motion of charge carriers, and a strong correlation between the dielectric properties and crystalline structure is observed. A dielectric relaxation below 90 K, commonly reported for rare-earth manganites crystals, was also observed in both samples. The results indicate that this relaxation is due to small-polaron tunnelling. Furthermore, polaron motion was observed to be affected by the magnetic transitions, structural properties and intrinsic anisotropies in TMO.

2. Experimental details

TMO powders were processed by high-energy ball milling for 12 h by using analytical graded Tb_4O_7 and MnO_2 precursors (Aldrich). The milled powders were calcined at 1200 °C for 1 h. The preparation of the powders and their structural characterizations will be published elsewhere. The calcined powders were ball remilled for 24 h and then isostatically pressed into circular pellets. The green pellets were sintered at 1400 °C for 5 h in either O_2 or Ar flux. The electrical conductance and susceptance of the samples were measured in the temperature range 10–300 K and frequency range 20 Hz–2 MHz using a Janis CCS-400H/204 cryogenic system and an Agilent E4980A LCR meter. Sputtered gold was used as electrodes. High-resolution x-ray powder diffraction (HR-XPD) and x-ray absorption fine-structure (XAFS) measurements were carried out at the Brazilian Synchrotron Light Laboratory (LNLS, Campinas). The wavelength of the incident beam ($\lambda = 1.549\,56$ Å) for HR-XPD was determined with a standard alumina powder (676a-NIST) and the data were acquired at room temperature in the range $2\theta = 18°$–$130°$. XAFS analyses were realized at the Mn K edge (6539 eV) for powdered remilled samples. The XAFS analyses were carried out in transmission mode with a Si(111) monochromator, leading to an energy resolution of about 2 eV [24], and at least three scans for each sample were collected and averaged to increase the quality of experimental data. Neutron diffraction patterns for remilled TMO samples were collected at 50 K using the E9 high-resolution powder diffractometer at the BERII reactor (Helmholtz-Zentrum-Berlin) in the angular range $2\theta = 20°$–$140°$ with a neutron wavelength of $\lambda = 1.7980$ Å [25].

3. Results and discussion

Figure 1 shows the temperature-dependent dielectric properties of TMO ceramics annealed in O_2 and Ar

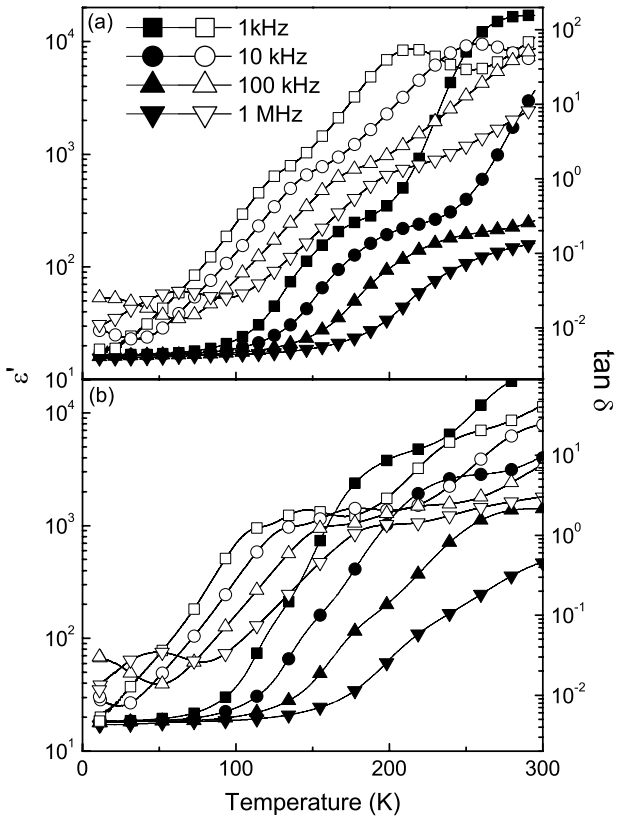

Figure 1. Temperature dependence of the dielectric constant and loss tangent for $TbMnO_3$ ceramics annealed in O_2 (a) and Ar (b) at some typical frequencies. Full symbols denote ε' experimental data; open symbols denote loss tangent experimental data. Lines are guides for the eyes.

atmospheres, from which two dielectric anomalies can be observed emerging in the temperature ranges ∼100–175 and ∼200–250 K, at 1 kHz. The loss tangent spectra of the sample annealed in Ar (figure 1(b)) exhibits an additional peak between 100 and 200 K. In both cases, the behaviours are dominated by a typical relaxation characteristic: $\varepsilon'(T)$ undergoes a steplike increase towards a large plateau value at higher temperatures, with marked dielectric dispersion. These anomalies are accompanied by broad relaxation peaks in the loss spectrum and the peak maximum position shifts towards higher temperatures with increasing frequency, indicating a thermally activated dynamics. Also, the peaks in tan δ become almost indistinct due to the exponential-like increasing background, a behaviour related to hopping conductivity. In fact, localized charge carriers hopping between potentials not only produce conductivity but also give rise to dipolar effects. An additional peak is also observed in the loss tangent below 90 K.

According to Wang *et al* [21], the dielectric behaviour of TMO ceramics is associated with the polarization of the charge carriers. It is well known that when charge carriers hop to the vicinity of grain boundaries or electrodes to form space charges, the relaxation of the space charges will result in an apparent giant dielectric constant due to the internal barrier-layer capacitance mechanism. A dielectric anomaly for the electric field direction **E** ∥ **c** was also observed at

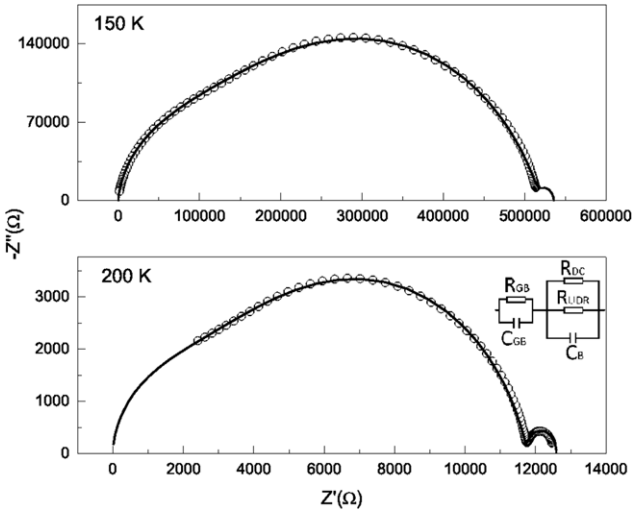

Figure 2. Complex impedance plots at 150 and 200 K for $TbMnO_3$ ceramics sintered in O_2 atmosphere. Open circles are the experimental data. Lines are the resultant fit obtained by using the equivalent circuit shown in the inset.

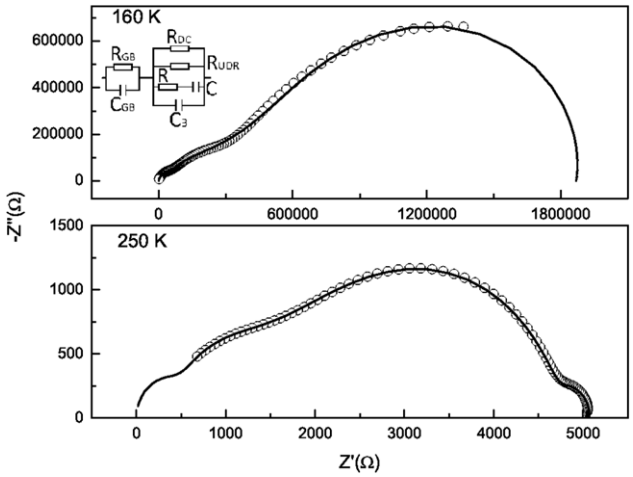

Figure 3. Complex impedance plots at 160 and 250 K for $TbMnO_3$ ceramics sintered in Ar atmosphere. Open circles are the experimental data. Lines are the resultant fit obtained by using the equivalent circuit shown in the inset.

∼130 K for TMO single crystals by Park *et al* [17], and attributed to thermal activation between the valence and conduction bands. They also observed a broad peak in the imaginary component of the dielectric constant below 100 K. This peak is superposed with a sharp peak at the lock-in temperature. This sharp peak is not present in our results due to the random orientation of crystals in the ceramics.

Regarding the inhomogeneous nature of polycrystals (due to the presence of grain boundaries, pores, cracks, etc), whether the dielectric anomalies come from the grain core or the grain boundary should first be determined. To evaluate this point, complex impedance spectra at different temperatures are presented in figures 2 and 3. It is noticeable that the spectra of both samples are composed of a small low-frequency arc and a distorted arc at intermediate and high frequencies. The experimental data was satisfactorily modelled by the

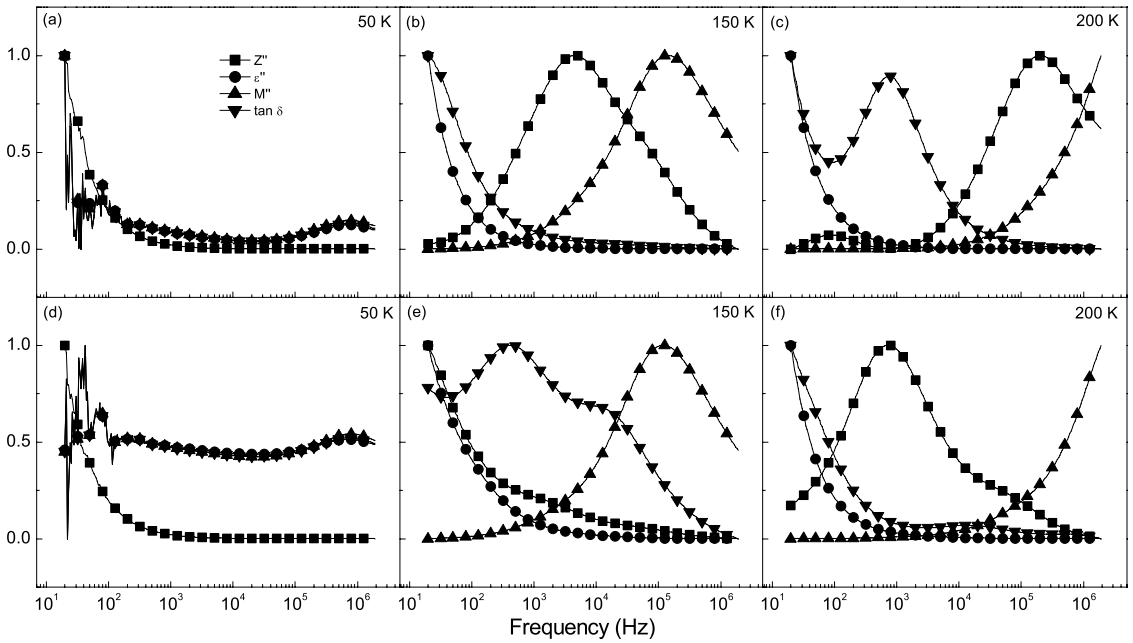

Figure 4. Simultaneous plots of normalized Z'', ε'', M'' and $\tan\delta$ at several temperatures for $TbMnO_3$ ceramics annealed in O_2 (a)–(c) and Ar (d)–(f). Lines are guides for the eyes.

circuit proposed by Lunkenheimer *et al* [27], shown in the inset of figure 2. The circuit consists of a leaky capacitor connected in series with the bulk sample. The intrinsic bulk response is given by the sum of the high-frequency dielectric constant $\varepsilon_\infty (C_B = \varepsilon_\infty C_0)$, dc conductivity and frequency-dependent ac conductivity, for which the 'universal dielectric response' (UDR) [28, 29] is used. The UDR is the most common approach to describe the conductivity of amorphous semiconductors and other disordered systems. It has been ascribed to relaxation caused by the motion of electrons, or atoms, hopping or tunnelling between equilibrium sites [29]. The intrinsic conductivity of the sample is given by

$$\sigma = \sigma_{dc} + \sigma_0 f^s, \tag{1}$$

where σ_{dc} is the dc conductivity, σ_0 is a constant, f is the frequency, and the exponent s is smaller than 1. From fitting, the calculated capacitances C_{GB} and C_B are of the order of 10^{-6} and 10^{-12} F. These values are usually associated to grain boundaries and bulk respectively [30]. With the values from the fittings, the dynamics of the process related to grain boundaries was analysed in the Arrhenius form

$$\tau = \tau_0 \exp(E_a/k_B T), \tag{2}$$

yielding activation energies of 227 meV for the sample annealed in O_2 and 237 meV for the sample annealed in Ar. With respect to the bulk response, in order to reproduce the observed behaviour of the sample annealed in Ar, a *RC* series branch was added to the equivalent circuit (inset in figure 3) to represent a localized relaxation process. This result is consistent with the analysis of simultaneous plots of normalized Z'', M'', ε'', and $\tan\delta$, shown in figure 4. It can be seen that for the sample annealed in O_2, the peaks in Z'' and M'' are partially superposed, indicating that the dielectric response has both localized and long-range characteristics, while the same peaks are much further apart in the Ar-annealed sample's spectra, indicating the predominance of localized relaxation processes.

It is worth noting that there is no observable peak in ε'' above 100 K, ruling out dipolar relaxation processes [31]. In fact, dielectric relaxation phenomena would give maxima both in the imaginary part of permittivity and of the dielectric modulus spectra, while a conductivity relaxation is indicated by the presence of a peak in M'' not accompanied by a peak in ε'' [32]. This fact corroborates the conclusions of Park *et al* [17] and Wang *et al* [21] that the observed dielectric anomalies for single and polycrystalline TMO are due to charge carriers.

In order to examine the behaviour of charge carries, the ac conductivity at 300 K of both samples is presented in figure 5. It can be seen that conductivity shows two plateaus and a strong rise between them, which appears at the same frequency region of the Z'' peak attributed to grain boundaries in figure 4. Therefore, the plateau at low frequencies is due to the conductivity of grain boundaries, while the second plateau is related to conduction in grain cores. Comparing the conductivity of both samples at the same temperature, it is noticeable that the sample annealed in O_2 is more conductive. It is also interesting to note that the grain boundary conductivity is more evident in the sample annealed in oxygen. Conductivity in oxides is usually attributed to the existence of defects in the material, particularly oxygen vacancies. Our results contradict this assumption, however, as the sample annealed in Ar atmosphere is expected to be oxygen deficient and hence present higher conductivity. Rietveld structural refinement of neutron diffraction data, figure 6, did not indicate the existence of oxygen vacancies in the Ar-annealed sample, while an oxygen excess of ~3.3%

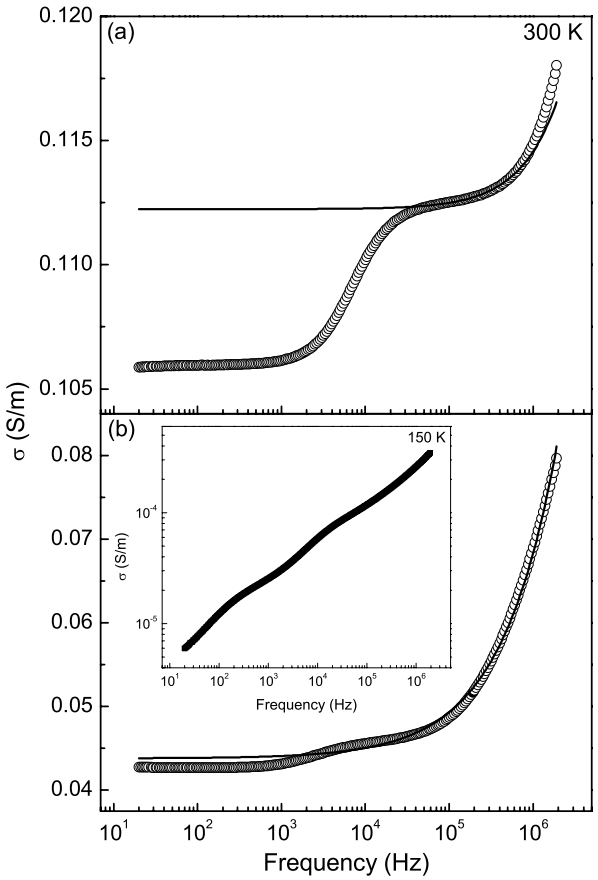

Figure 5. Ac conductivity at 300 K for $TbMnO_3$ ceramics annealed in O_2 atmosphere (a) and Ar atmosphere (b). Open circles are the experimental data; solid lines are the fitting results according to equation (1). The inset displays $\log \sigma_{ac}$ versus $\log f$ at 150 K for $TbMnO_3$ ceramics annealed in Ar.

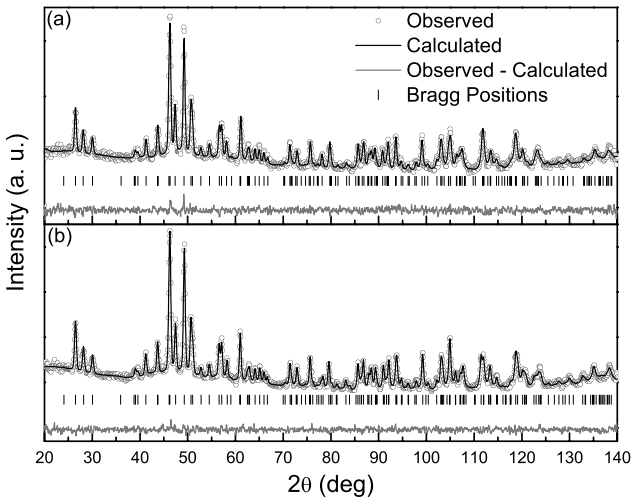

Figure 6. Neutron powder diffraction at 50 K and Rietveld refinement of $TbMnO_3$ ceramics sintered in (a) O_2 ($\chi^2 = 0.87$, $R_p = 20.6$, $R_{wp} = 18.9$, $R_{exp} = 20.2$) and (b) Ar ($\chi^2 = 0.78$, $R_p = 16.1$, $R_{wp} = 15.3$, $R_{exp} = 17.4$) atmosphere. Space group *Pbnm* was used in the refinement of both samples' data.

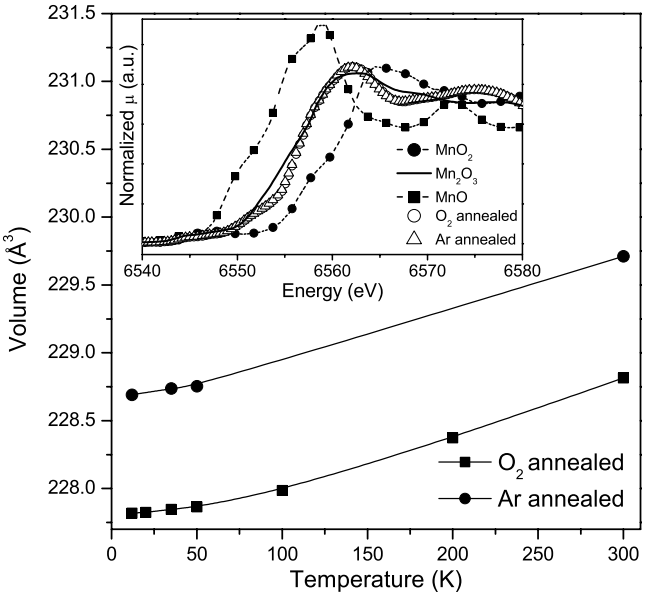

Figure 7. Temperature dependence of the unit cell volume, calculated from HR-XPD data, for $TbMnO_3$ ceramics annealed in O_2 and Ar atmospheres. The inset displays XAS results for both samples, to be compared with MnO, MnO_2 and Mn_2O_3 standards.

was detected in the O_2-annealed sample. Oxygen excess could lead to a change in valence of the Mn ions, which would affect the electrical properties. However, XANES results, presented in the inset of figure 7, show that Mn ions, despite the different atmosphere (oxidative or reductive), showed no oxidation changes. TMO XAFS spectra for Ar and O_2 sintered samples, and the Mn_2O_3 (Mn^{3+}) standard are strongly overlapped, as expected for stoichiometric TMO. In this way, one concludes that the dielectric anomaly observed in the temperature range 100–175 K is caused neither by the samples' microstructure nor the presence of defects, therefore being, in fact, intrinsic to TMO.

The inset of figure 5(b) shows $\log \sigma$ versus $\log f$ at 150 K for the sample sintered in Ar atmosphere, from which deviations from linearity can be noticed. It has been demonstrated [33] that when conducting species move between inequivalent sites, 'bumps' can be observed in $\sigma(f)$. The motion of charged species may involve several distinguishable jump processes, each governed by a different activation energy. It has also been demonstrated [34] that in such cases a polarization arises from the inequalities in jump probabilities, which is related to the *RC* branch in the equivalent circuit in the inset of figure 3. From the impedance data, it is noticeable that the effect of the existence of inequivalent sites is less evident in the sample sintered in O_2. This fact can be related to the oxygen excess in this sample. These extra oxygen ions can modify the band structure of the material and create a 'smoother' conduction path. Structural features might also play an important role. Actually, it is known that changes in structural characteristics such as the c/a ratio and cell volume can produce overlapping bands (or stop the overlapping of two bands, in case of expansion) inducing a metal–insulator transition [35]. As can be seen in figure 7, there is a significant difference in unit cell volume between the samples, with the Ar-annealed sample having

Table 1. Parameters used when fitting the conductivity data in figure 6 with equation (1).

	T (K)	σ_{dc}	σ_0	s
O_2-annealed	100	1.57×10^{-7}	5.96×10^{-9}	0.60
	150	2.89×10^{-5}	6.51×10^{-7}	0.43
	200	1.45×10^{-3}	3.27×10^{-7}	0.63
	250	1.95×10^{-2}	4.26×10^{-9}	0.98
	300	0.11	4.03×10^{-9}	0.96
Ar-annealed	100	1.57×10^{-7}	5.76×10^{-9}	0.60
	150	3.32×10^{-6}	1.99×10^{-6}	0.35
	200	1.25×10^{-4}	1.87×10^{-5}	0.37
	250	3.11×10^{-3}	5.06×10^{-5}	0.40
	300	0.04	3.19×10^{-6}	0.65

a larger cell volume. The fact that ions are more closely positioned might favour charge conduction and be one of the factors explaining why the O_2-annealed sample is more conductive. In fact, density functional theory calculations [26] show that there is a strong hybridization between Tb 4f, Mn 3d and O 2p states, and the relative position between ions might affect the electronic band structure. As would be expected, these structural differences affect the magnetic properties of the sample as well (magnetic data and their analyses will be published elsewhere).

The conductivities of the grain cores of both samples were fitted with equation (1), the obtained fitting parameters at a few selected temperatures are presented in table 1. One can notice that all the parameters are very sensitive to temperature. The exponent s, in particular, does not exhibit a single tendency in the whole temperature range, suggesting that UDR alone cannot account for all the observed conductivity's features.

In hopping conduction, the nearest-neighbour hopping obeys the Arrhenius-like law

$$\sigma_{dc} = \sigma_1' \exp(-E_a/k_B T), \tag{3}$$

where σ_1' is a constant, E_a is the activation energy, k_B the Boltzmann constant, and T the absolute temperature. Mott [36] first pointed out that at low temperatures the most frequent hopping process would not be to a nearest neighbour. Then, Mott's variable-range-hopping (VRH) conductivity sets in. The VRH conduction mechanism can be described by the equation

$$\sigma_{dc} = \sigma_1 \exp[-(T_0/T)^{1/4}], \tag{4}$$

where σ_1 and T_0 are constants and T_0 is given by [37]

$$T_0 = 24/[\pi k_B N(E_F)\xi^3], \tag{5}$$

where $N(E_F)$ is the density of localized states at the Fermi level, and ξ is the decay length of the localized wavefunction. This approach has been used in the interpretation of conductivity data of several oxides [37–39], including $DyMnO_3$ [22].

The temperature dependence of the dc conductivity of both samples, obtained by equation (1), was analysed with equations (3) and (4). From Arrhenius plots (figure 8), the

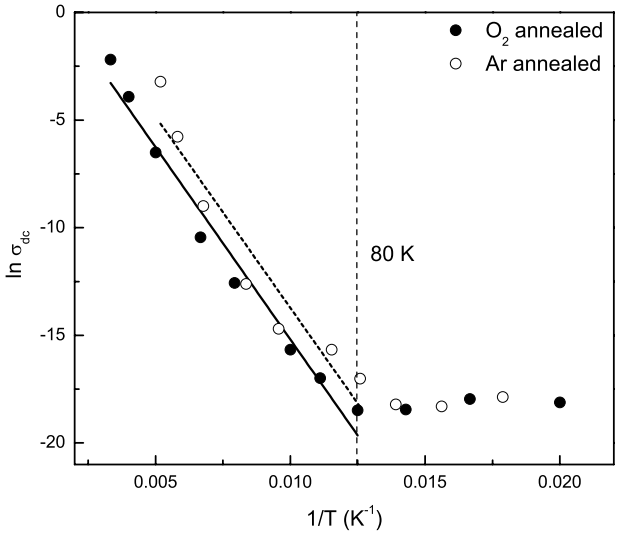

Figure 8. Arrhenius plot of σ_{dc}. Symbols are the experimental data; solid and dashed lines are fitting results according to equation (3) for $TbMnO_3$ ceramics annealed in O_2 and in Ar respectively. The vertical dashed line shows the position $T = 80$ K at which a dielectric relaxation becomes evident (see text).

calculated conductivity's activation energy is 154 meV for the O_2-annealed sample and 133 meV for the sample annealed in Ar. However, a slightly better agreement was achieved by using equation (4). Mott's VRH mechanism gives two relations [36]

$$W = 3/[4\pi R^3 N(E_F)], \tag{6}$$

$$R = \xi^{1/4}/[8\pi N(E_F) k_B T]^{1/4}, \tag{7}$$

where W and R are the hopping energy and hopping range respectively. According to equations (5)–(7), we obtain

$$W = 1.6 k_B T_0^{1/4} T^{3/4}, \tag{8}$$

$$R = 0.27\xi \left(\frac{T_0}{T}\right)^{1/4}. \tag{9}$$

The obtained values of T_0 are 9.68×10^8 K and 5.77×10^8 K for the samples annealed in O_2 and Ar respectively. The occurrence of VRH might be related to the existence of inequivalent sites, as evidenced by conductivity and complex impedance data analyses. The dependence of W with T is plotted in the inset of figure 9. Further experiments, such as EPR or band-structure calculations, are necessary to determine $N(E_F)$, ξ, and R. It is interesting noting that both Arrhenius and VRH mechanism analyses gave higher values of activation energy for the sample annealed in O_2 atmosphere, which indicates that barriers between sites are higher in this sample. In this case, the lower conductivity observed in samples sintered in Ar can be related to inequivalent sites trapping the charge carriers.

Below 100 K both M'' and ε'' spectra present maxima, indicating the occurrence of a dielectric relaxation phenomenon of dipolar nature. Figure 10 shows the complex plane plot at 40 K of the dielectric constant of the O_2-annealed sample. It is composed of a depressed semicircle and a

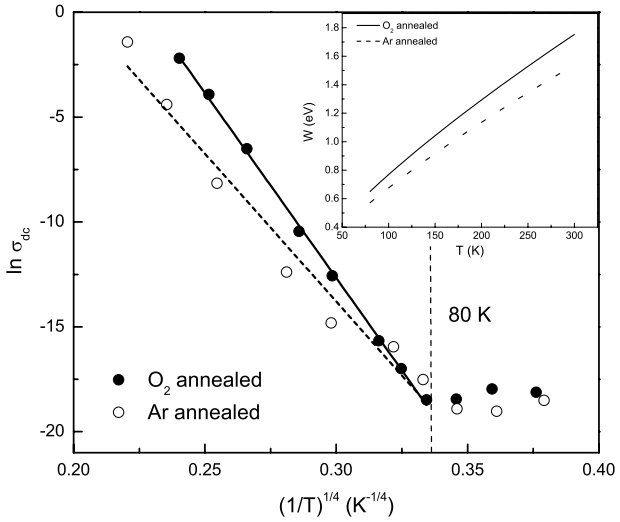

Figure 9. Temperature dependence of dc conductivity. Symbols are the experimental data; solid and dashed lines are fitting results according to Mott's variable-range-hopping mechanism, equation (4), for $TbMnO_3$ ceramics annealed in O_2 and Ar respectively. The inset shows the hopping energy versus temperature according to equation (6). The vertical dashed line shows the position $T = 80$ K at which a dielectric relaxation becomes evident (see text).

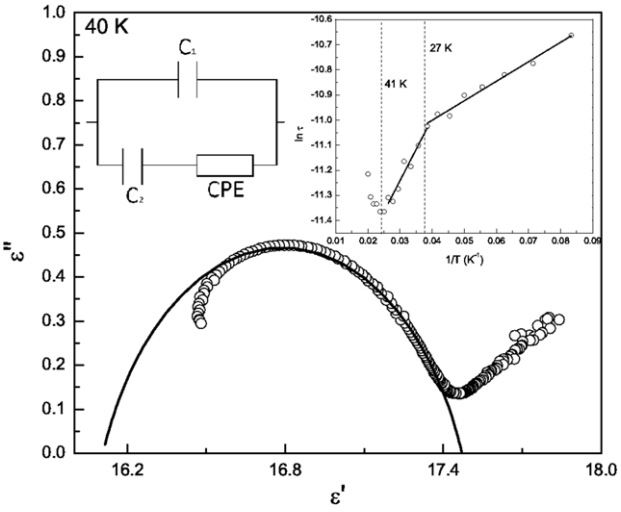

Figure 10. Cole–Cole plot at 40 K for $TbMnO_3$ ceramics annealed in O_2. Open circles are the experimental result; the solid line is the fitting result according to the equivalent circuit shown in the inset in the upper left corner. The inset in the upper right corner displays the temperature dependence of the relaxation time τ. Solid lines are the fitted result according to the Arrhenius' relation, equation (2). Vertical dashed lines mark the position of the AFM transition (41 K) and the lock-in temperature (27 K).

low-frequency tail, indicating high losses in the material. The semicircle could be satisfactorily fitted with the Cole–Cole equation [40]

$$\varepsilon = \varepsilon_\infty + (\varepsilon_s - \varepsilon_\infty)/[1 + (i\omega\tau)^{1-\alpha}], \qquad (10)$$

where ε_s is the static permittivity, τ is the mean relaxation time, and α represents the degree of distribution of relaxation times. From the fitting, the mean relaxation time was calculated at several temperatures in the range 12–50 K and its temperature dependence was analysed with the Arrhenius relation (equation (2)). This result is shown in the inset of figure 10. It can be clearly seen that the relaxation dynamics changes in the vicinity of 41 and 27 K. These are, respectively, the temperatures at which an incommensurate sinusoidal AFM ordering of Mn^{3+} moments appears and the incommensurate–commensurate transition occurs. The latter is also related to the appearance of ferroelectricity in TMO. The calculated activation energies are 2.13 meV between 40 and 26 K and 0.67 meV between 26 and 12 K.

It is worth mentioning that from figures 8 and 9 it can be noticed that σ_{dc} becomes practically independent of temperature below ∼80 K, in the temperature range where the aforementioned dielectric relaxation appears. The two phenomena might have the same origin. It is known that small-polaron tunnelling becomes independent of temperature at low temperatures (far below the Debye temperature). Localization of charge carriers can lead to the formation of small polarons if the presence of the carrier produces a local lattice distortion in such a way that the total energy of the system (electronic + distortion) is thereby lowered by an amount W_p, the polaron energy. Polaron formation is usually attributed to the trapping of charge carriers in randomly distributed structural defects. However, if every atomic site can in principle act as a trapping site for carriers, the centres between which polarons move are not randomly distributed spatially, thereby hopping between nearest neighbours or possibly next-nearest neighbours is expected. The effect of a non-random distribution of centres on small-polaron motion would be to introduce a peak in the dielectric loss function ε'', if the hopping length is comparable to the first few interatomic spacings [29]. Therefore small-polaron tunnelling can explain the observed behaviour of conductivity and the dielectric relaxation below ∼80 K. At low temperatures the relaxation time of small-polaron tunnelling is given by [29]:

$$\tau = \tau_0 \exp\left(\frac{W_h}{\frac{1}{4}\hbar\omega_0}\right) \exp(2\beta R), \qquad (11)$$

where W_h is the activation energy for polaron transfer, ω_0 is the vibrational frequency describing the lattice distortion (phonon frequency), β is the polarizability of a pair of sites and R is the distance between sites. Far-infrared spectroscopy results have demonstrated that a strong spin–phonon coupling exists in TMO [41], and the frequencies of some phonon modes exhibit a strong temperature dependence. Moreover, ion displacements are assumed to play a major role in the occurrence of ferroelectricity in TMO [42, 43]. These facts suggest that the parameters ω_0 and R, in equation (11), are affected by the magnetic transitions, explaining the behaviour observed in figure 10. One last question remains: can small-polaron tunnelling justify the appearance of the dielectric relaxation along a specific crystalline direction? In anisotropic crystals, the electron–phonon interaction is also anisotropic, which makes polarons motion more probable along a specific crystalline direction [44]. In fact, TMO exhibits

high electronic and bonding anisotropies, as demonstrated by polarization-dependent far-infrared spectroscopy [41] and x-ray absorption spectroscopy [45–47] measurements, consequently leading to the existence of a more favourable tunnelling direction.

4. Conclusions

Three dielectric anomalies have been observed in the temperature range 10–300 K for TMO ceramics. Two of them appear above 100 K and are caused by the thermal activation of charge carriers and their motion in grain cores (∼100–175 K) and grain boundaries (above 200 K). The results evidenced that, in grain cores, carriers move between inequivalent sites according to Mott's VRH mechanism. The effects of the inequivalent sites, and consequently, the electrical and dielectrical properties of the samples are highly dependent on their structural properties. As the temperature is lowered, the carriers become trapped, forming small polarons, which are responsible for the dielectric relaxation that appears below ∼90 K, commonly observed in rare-earth manganites crystals. There is evidence of an anisotropic electron–phonon interaction affecting the small-polaron tunnelling—this fact is responsible for the low-temperature relaxation being observed only along a specific crystalline direction. It is also worth mentioning that the dielectric anomaly due to the motion of charge carriers in the grain boundaries is the only one of extrinsic origin, while the anomalies related to carrier motion in the grain cores and small-polaron tunnelling are intrinsic to TMO.

Acknowledgments

The authors would like to thank the Brazilian Synchrotron Light Laboratory for HR-XPD and XAFS analyses, and Helmholtz-Zentrum-Berlin for neutron diffraction analyses. This research is sponsored by CNPq (Proc. 305129/2010-4), CAPES (PROCAD 082/2007), Fundação Araucária de Apoio ao Desenvolvimento Científico e Tecnológico do Paraná (Prot. 22825, 24202, and 22870), and FAPESP (Proc. 2008/04025-0) Brazilian research funding agencies. GSD and LGDS also thank CNPq for fellowships.

References

[1] Scott J F 2007 *Science* **315** 954
[2] Hill N A 2000 *J. Phys. Chem.* B **104** 6694
[3] Kimura T, Goto T, Shintani H, Ishizaka K, Arima T and Tokura Y 2003 *Nature* **426** 55
[4] Hur N, Park S, Sharma P A, Ahn J S, Guha S and Cheong S-W 2004 *Nature* **429** 392
[5] Lawes G *et al* 2005 *Phys. Rev. Lett.* **95** 087205
[6] Kimura T, Lashley J C and Ramirez A P 2006 *Phys. Rev.* B **73** 220401(R)
[7] Yamasaki Y, Miyasaka S, Kaneko Y, He J-P, Arima T and Tokura Y 2006 *Phys. Rev. Lett.* **96** 207204
[8] Taniguchi K, Abe N, Takenobu T, Iwasa Y and Arima T 2006 *Phys. Rev. Lett.* **97** 097203
[9] Kimura T, Lawes G and Ramirez A P 2005 *Phys. Rev. Lett.* **94** 137201
[10] Tokura Y and Seki S 2010 *Adv. Mater.* **22** 1554
[11] Quezel S, Tcheou F, Rossat-Mignod J, Quezel G and Roudaut E 1977 *Physica* B **86–88** 916
[12] Goto T, Kimura T, Lawes G, Ramirez A P and Tokura Y 2004 *Phys. Rev. Lett.* **92** 257201
[13] Sergienko I A and Dagotto E 2006 *Phys. Rev.* B **73** 094434
[14] Mostovoy M 2006 *Phys. Rev. Lett.* **96** 067601
[15] Katsura H, Nagaosa N and Balatsky A V 2005 *Phys. Rev. Lett.* **95** 057205
[16] Yamasaki Y, Sagayama H, Goto T, Matsuura M, Hirota K, Arima T and Tokura Y 2007 *Phys. Rev. Lett.* **98** 147204
[17] Park Y A, Song K M and Hur N 2008 *J. Korean Phys. Soc.* **53** 3356
[18] Schrettle F, Lunkenheimer P, Hemberger J, Ivanov V Yu, Mukhin A A, Balbashov A M and Loidl A 2009 *Phys. Rev. Lett.* **102** 207208
[19] Kagawa F, Muchizuki M, Onose Y, Murakawa H, Kaneko Y, Furukawa N and Tokura Y 2009 *Phys. Rev. Lett.* **102** 057604
[20] Kagawa F, Onose Y, Kaneko Y and Tokura Y 2011 *Phys. Rev.* B **83** 054413
[21] Wang C C, Cui Y M and Zhang L W 2007 *Appl. Phys. Lett.* **90** 012904
[22] Yang J *et al* 2012 *Appl. Phys. Lett.* **101** 222904
[23] Hong F, Cheng Z X, Zhang S J and Wang X L 2012 *J. Appl. Phys.* **111** 034104
[24] Tolentino H C N, Ramos A Y, Alves M C M, Barrea R A, Tamura E, Cezar J C and Watanabe N 2001 *J. Synchrotron Radiat.* **8** 1040
[25] Többens D M, Strüßer N, Knorr K, Mayer H M and Lampert G 2001 *Mater. Sci. Forum* **378–381** 288
[26] Lu-Gang C, Fa-Min L and Wen-Wu Z 2010 *Chin. Phys.* B **19** 097101
[27] Lunkenheimer P, Bobnar V, Pronin A V, Ritus A I, Volkov A A and Loidl A 2001 *Phys. Rev.* B **66** 052105
[28] Jonscher A K 1977 *Nature* **267** 673
[29] Elliot S R 1987 *Adv. Phys.* **36** 135
[30] Hodge I M, Ingram M D and West A R 1976 *J. Electroanal. Chem.* **74** 125
[31] Jonscher A K 1999 *J. Phys. D: Appl. Phys.* **32** R57
[32] Gerhardt R 1994 *J. Phys. Chem. Solids* **12** 1491
[33] Wong T and Brodwin M 1980 *Solid State Commun.* **36** 503
[34] Franceschetti D R and Shipe P C 1984 *Solid State Ion.* **11** 285
[35] Mott N F 1990 *Metal–Insulator Transitions* 2nd edn (London: Taylor and Francis)
[36] Mott N F and Davis E A 1979 *Electronic Processes in Non-Crystalline Materials* (Oxford: Clarendon)
[37] Zhang L and Tang Z J 2004 *Phys. Rev.* B **70** 174306
[38] Kastner M A *et al* 1988 *Phys. Rev.* B **37** 111
[39] Ang C, Jing Z and Yu Z 1999 *J. Phys.: Condens. Matter* **11** 9703
[40] Cole K S and Cole R H 1941 *J. Chem. Phys.* **9** 341
[41] Schmidt M, Kant Ch, Rudolf T, Mayr F, Mukhin A A, Balbashov A M, Deisenhofer J and Loidl A 2009 *Eur. Phys. J.* B **71** 411
[42] Malashevich A and Vanderbilt D 2008 *Phys. Rev. Lett.* **101** 037210
[43] Xiang H J, Wei S-H, Whangbo M-H and Da Silva J L F 2008 *Phys. Rev. Lett.* **101** 037209
[44] Kornilovitch P E 1999 *Phys. Rev.* B **59** 13531
[45] Chen J M *et al* 2009 *Appl. Phys. Lett.* **94** 044105
[46] Wu K H *et al* 2010 *J. Phys.: Conf. Ser.* **200** 012227
[47] Chen J M *et al* 2010 *Phys. Rev.* B **82** 094442